PLANETARY SCIENCE

Intense subaerial weathering of eolian sediments in Gale crater, Mars

Jiacheng Liu[1,2], Joseph R. Michalski[1,2]*, Mei-Fu Zhou[1,3]

After over 8 years of successful surface operations on Mars, the Curiosity rover has revealed much about the environment in Gale crater. Despite early observations of a lacustrine environment, few of the subsequent deposits exhibit demonstrable lacustrine character. We suggest instead that most of the stratigraphic section explored to date can be best explained as eolian and/or volcaniclastic sediments subaerially chemically weathered by acidic precipitation in a reduced atmosphere. Most of the deposits in Gale crater seemingly did not form in an ancient lake, but the results nonetheless shed considerable light on ancient climate, environmental change, and the astrobiology of Mars. Discoveries by Curiosity provide a critical piece to Mars' global alteration puzzle.

INTRODUCTION

Altered, clay mineral–rich rocks found within Gale crater by the Curiosity rover clearly trace interactions between the ancient crust and surface or near-surface water, with major implications for past climate and habitability. Gale crater was chosen as the landing site because of the likelihood of discovering lacustrine rocks, and expectedly, evidence for lake deposits in the floor of the crater has received substantial attention (*1*–*4*). However, after 8 years of surface exploration, the rocks that are decidedly lacustrine in origin represent only a small fraction of the geologic record so far explored.

Although surface operations have revealed significant evidence for fluid-rock interactions [e.g., (*2*, *5*)], we argue that most of this evidence (especially, the "mudstone") actually points to subaerial chemical weathering of eolian deposits rather than a lacustrine environment. If true, then this elucidates the connection between the properties of Gale crater deposits observed in situ and the context observed from orbit (*6*, *7*), which favors eolian deposition (*8*–*10*). The weathering connection in Gale crater opens up an invaluable window into a global-scale weathering process, resulting in the formation of Al- and Si-rich alteration products and Fe mobility observed throughout the ancient surface via remote sensing (*11*).

RESULTS AND DISCUSSION

A transient and limited lacustrine environment in Gale crater

The Yellowknife Bay formation, exposed near Curiosity's landing site, contains a layer, ~2 to 4 m in vertical thickness, of very fine-grained (below the resolution of the microscopic imager of ~14 μm per pixel where grain detection requires multiple pixels), clay mineral–rich sediment similar to lacustrine deposits on Earth (*3*). Associated deposits, such as conglomerates (*12*), demonstrate high-energy aqueous processes but are themselves not lacustrine. The Yellowknife Bay lacustrine rocks exposed at −4520-m elevation represent less than 1% of the >400-m-thick stratigraphic section explored to date (Fig. 1). The majority of the stratigraphic section corresponds to sandstone and interbedded mudstone-sandstone, which are intensely weathered but likely not lacustrine in origin based on the suite of sedimentary structures, mineralogy, and geochemical trends observed as a geological formation.

The occurrence of fine laminations of mudstones in the Murray formation could indicate episodic deposition in a low-energy, lacustrine setting. However, ubiquitous cross-bedded sandstones (fig. S1) interbedded with the laminated mudstones (*13*) are difficult to explain through lacustrine processes alone, instead requiring several episodes of eolian-dominated activity. The fine laminations might actually have formed through airfall deposition of dust or likely volcanic ash. Interbedded, reworked, and draping eolian sand and volcanic ash deposits could account for the large variation of dips of sediment layers (fig. S2) even within the same unit (*14*). The sanidine (*15*), tridymite (*16*), and high Zn and Ge concentrations (*17*) indicate hydrothermal processes. Together, these materials are best explained as fine-grained airfall deposits partially reworked by eolian processes and altered in situ.

Quantification of weathering intensity on Mars

Aluminous dioctahedral smectite occurring throughout the ~400-m-thick Murray formation is considered evidence for open-system aqueous alteration of basaltic detritus in the putative lake (*5*). The chemical alteration of fine-grained sedimentary rocks in an open system before or during their emplacement is also suggested at Gale crater by Mangold *et al.* (*18*). These clay mineral–bearing sandstones could alternatively represent chemically weathered eolian deposits after their emplacement in a subaerial environment. The chemical index of alteration (CIA) [$CIA = 100 * Al_2O_3/(Al_2O_3 + CaO + Na_2O + K_2O)$] is discussed and applied to be a first-order estimate for weathering intensity on Mars (*18*–*22*). Quantitative mineralogical abundances are used to exclude the Ca, Na, and K contributed by salts (*21*, *23*) when x-ray diffraction (XRD) data are available.

However, CIA used to interpret alteration is fundamentally dependent on weathering of feldspars (*24*), the relative weathering rate of which is efficient under neutral or slightly acidic environments typical on this planet (*25*). While this assumption works well for many environments on Earth, the weathering index might not apply to the setting in Gale crater, leading to confusion about the degree of weathering in a uniquely Martian setting.

CIA is a powerful parametrization of weathering intensity on Earth, because the protoliths and surface water conditions are well understood. Ultimately, any chemical proxy of alteration is a reflection of the relative rate of chemical breakdown of mineral phases and

[1]Research Division for Earth and Planetary Science, The University of Hong Kong, Hong Kong, China. [2]Laboratory for Space Research, The University of Hong Kong, Hong Kong, China. [3]School of Earth Resources, China University of Geosciences, Wuhan, China. *Corresponding author. Email: jmichal@hku.hk

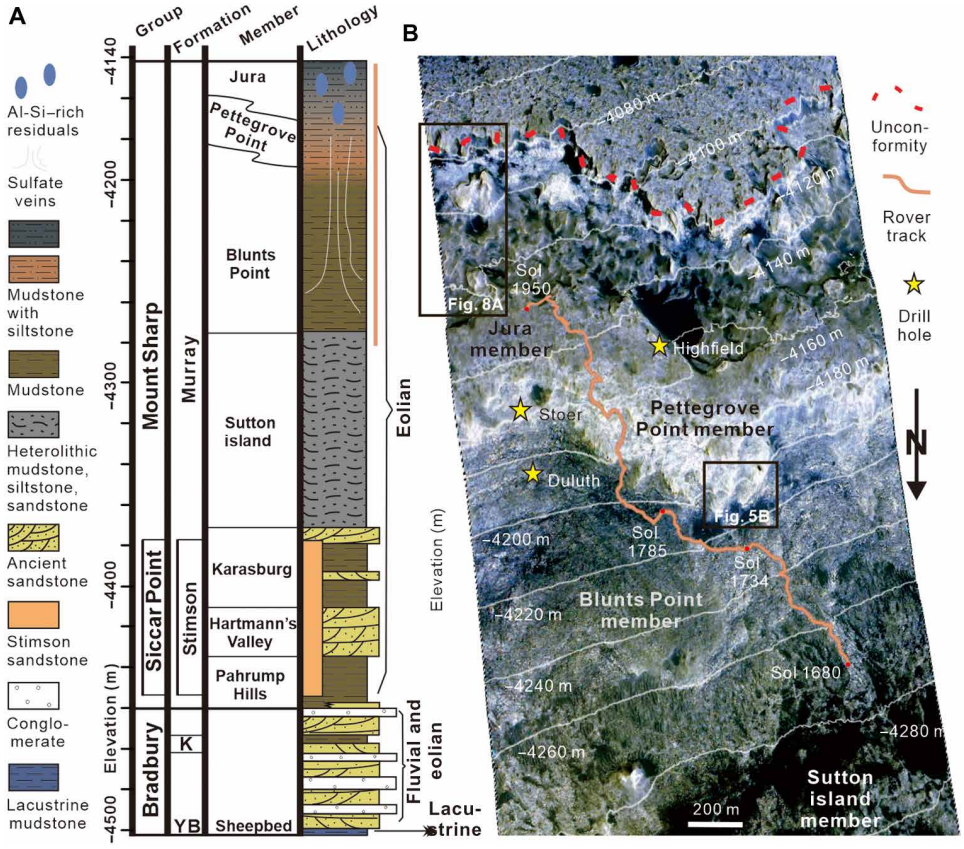

Fig. 1. The stratigraphic column and Curiosity rover's traverse in Gale crater. (**A**) Stratigraphic column of the rocks in Gale crater, which is modified from Fedo *et al.* (*64*). (**B**) High Resolution Imaging Science Experiment (HiRISE) image (ESP_045293_1755_COLOR) of Mars Science Laboratory (MSL) traverse between the Sutton island and Jura members. The solid orange line is the traverse between Sol 1680 and Sol 1950. Elevation increases from the bottom of the HiRISE image to the top, and the orange traverse line is also shown for reference to the right of the stratigraphic column.

glasses, as a function of not only the phase identity but also the texture and grain size of each phase. Chemical weathering in Gale crater cannot be accurately evaluated by the CIA for several reasons. First, the Fe/Mg-rich mafic minerals, which contribute a much larger proportion to the Martian environment than is typical for studied areas on Earth (*26*), are weathered more efficiently than feldspars (*27*). However, CIA does not take Mg and Fe into consideration. Second, the surface water on Mars is widely considered to be acidic (*25*, *28*, *29*), different from the neutral or slightly acidic waters typical on this planet. The acidic environment not only markedly increases the weathering rate of olivine compared to feldspars (*29*) but also affects the mobility of alkaline elements (e.g., potassium) (*30*). Third, ubiquitous sulfates (*13*, *31*) and chlorides (*32*) occur as pervasive, thin veins (fig. S3), which can affect interpretations of bulk chemistry in Gale crater. Ca and Na in salts can change the value of CIA (*21*, *23*). In addition, unavoidable K-metasomatism during diagenesis (*33*) affects the value of CIA. CIA should be reconsidered when applied to Mars. Any index of weathering useful for Mars must measure chemical mobility from phases likely to be present, and the conditions of chemical mobility must be tuned to the Martian setting (e.g., pH and redox).

The concentrations of SiO_2 and Al_2O_3 are highly correlated [coefficient of determination (R^2) = 0.95] in altered rocks (from Sol 1700 to Sol 2300) in Gale crater (Fig. 2A), suggesting that Si and Al were either synchronously added or retained during alteration. The positive correlations among SiO_2, Al_2O_3, and generally immobile TiO_2 (Fig. 2B and fig. S4) strongly suggest that Si and Al were concentrated as a residual material due to immobility. On the other hand, the poor correlation between SiO_2 and Al_2O_3 in silicate amorphous materials (Fig. 2C) (*34*) refutes the hypothesis of synchronous addition of Al and Si during sedimentation and diagenesis proposed by Thompson *et al.* (*35*). The siliceous and aluminous materials are more consistent as residual products.

The negative correlation between abundances of mafic minerals and Si-rich amorphous materials (Fig. 2D) suggests that the amorphous materials are mainly formed by alteration of mafic minerals (*36*). The negative correlation between Fe and Mg and SiO_2 in amorphous materials (fig. S5A) suggests leaching of Fe and Mg during alteration. The positive correlation between amorphous abundance and proportion of Si in the amorphous materials (fig. S5B) is consistent with a weathering process rather than a sedimentary mechanism (*36*).

Although Si is mobile during the alteration of basalts under a wide range of pH-T conditions (*36*), the solubility of silica is strongly limited by aqueous salts (*37*). There is a decrease of up to 95% solubility in a solution saturated with Ca/Mg chlorides or sulfates (*37*). This may be why Si was nearly immobile and occurs as amorphous materials in the upper parts of basaltic sequences weathered by H_2SO_4-HCl–type solutions (*30*, *38*, *39*). The acidic conditions may

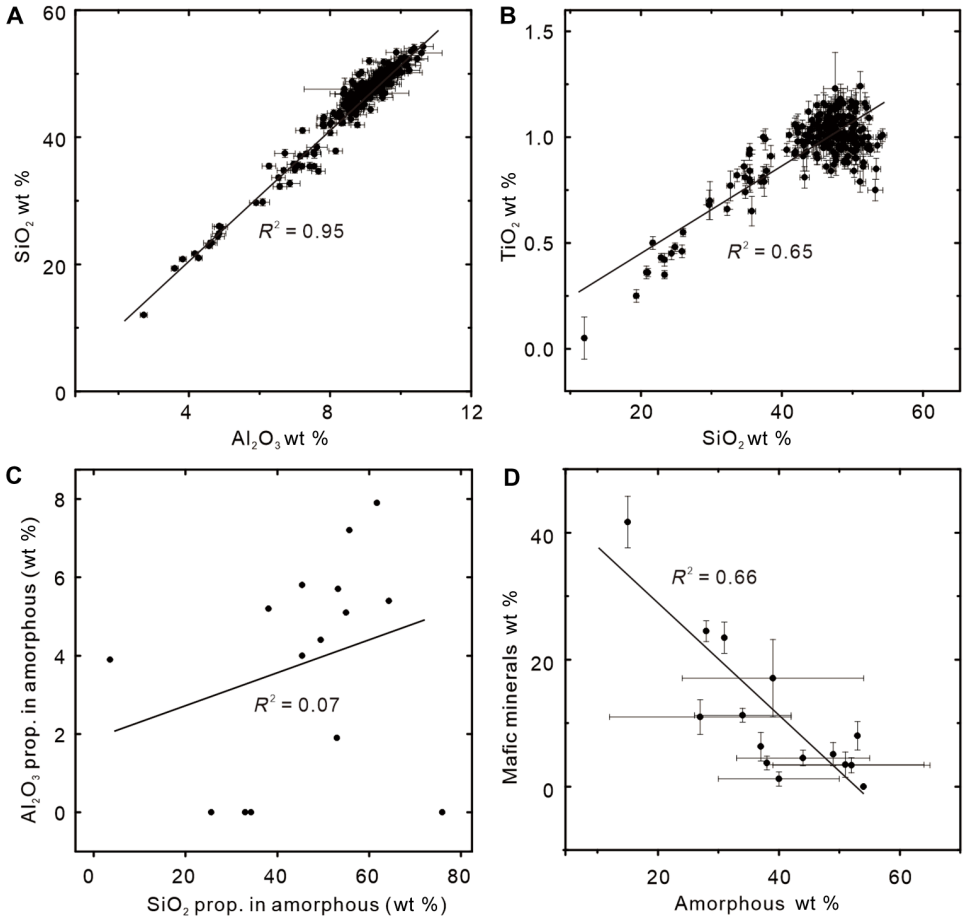

Fig. 2. Immobile Si and Al in Gale crater. (**A**) Positive correlation between SiO_2 and Al_2O_3 for all alpha particle x-ray spectrometer (APXS) analyzing results from Sol 1700 to Sol 2301. wt %, weight %. (**B**) Positive correlation between SiO_2 and TiO_2 for the same samples. (**C**) Poor correlation between the proportions of Si and Al in amorphous materials. (**D**) Negative correlation between abundances of mafic minerals and amorphous materials. Data in (C) and (D) are adapted from Rampe *et al.* (*34*).

be created by the volcanic outgassing of SO_2 and HCl, which make the precipitation and surface water on Mars very acidic (*30*, *40*–*42*).

Although the solubility of Al can be enhanced under acidic conditions (*25*), the dissolution rate of primary aluminosilicates (e.g., plagioclase) is still the lowest among the minerals typical of basalts (*27*). Because of the low mobility of Al and Si compared to other major elements, Martian mafic sediments become aluminous and siliceous during acidic weathering and leaching (*30*). Weathering by acidic, H_2SO_4-HCl–bearing solutions in relatively low water/rock conditions should result in residual Al and Si (*30*). This association between Si and Al can explain the positive correlation between the CIA and concentration of SiO_2 on Mars (*1*), in contrast to the negative correlation on Earth (*36*).

The molar proportion of Al alone is a good measure of weathering intensity under acidic conditions, which take all mobile elements into consideration, including Mg and Fe contributed by weathering of olivine and pyroxene. To diminish the influence of pervasive salts, we directly exclude the molar contribution from sulfur and halogens and their combined alkaline (earth) elements in the molar sum. The method is efficient and useful, especially when mineralogical data are lacking. We calculate the weathering intensity using the equation

$$\text{The molar proportion of } Al_2O_3 = \text{mol } Al_2O_3 / (\text{molar sum of all major elements except S, Cl, and Br} - (\text{mol } SO_3 + 0.5 * \text{mol Cl} + 0.5 * \text{mol Br}))$$

Evidence for subaerial weathering

The ratio of Ti to Al, which can be used to discriminate lithological changes in the protolith (*24*), is nearly constant throughout the section (Fig. 3A and fig. S4). The indication of homogeneous composition is an important first-order criterion for the exploration of a paleosol hypothesis (*43*). The slight decrease in TiO_2/Al_2O_3 in the uppermost section suggests leaching of Ti due to extreme acidity at the highest parts of the section (Fig. 3A) (*29*). The upward increasing molar proportions of Al_2O_3 and SiO_2 in the stratigraphic section (Fig. 3A) strongly indicate the loss of other major elements (e.g., Mg^{2+}, Ca^{2+}, and alkali elements) throughout the entire section. The upward decreasing trends of MgO/Al_2O_3, P_2O_5/Al_2O_3, and Zn/Al_2O_3 ratios are consistent with the leaching interpretation (Fig. 3B). Critically, the upward decreasing Fe_2O_3/Al_2O_3 ratios suggest leaching of Fe. Fe and Al have similar chemical behavior in oxidized fluids (*25*); therefore, the separation of Fe from Al strongly implicates weathering by reduced fluids (*9*).

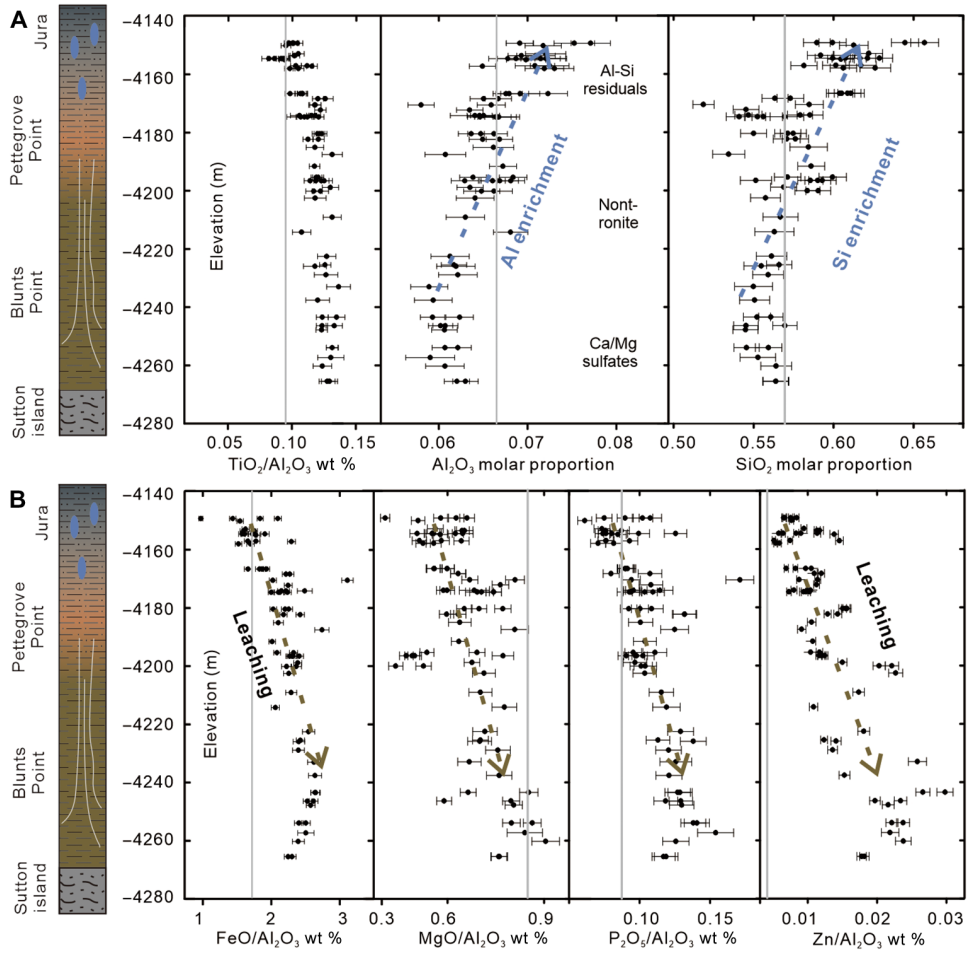

Fig. 3. Geochemical evidence for a paleo-weathering sequence. The upward increasing trends of Al_2O_3 and SiO_2 with constant TiO_2 (**A**) and the upward decreasing trends of MgO/Al_2O_3, P_2O_5/Al_2O_3 and Zn/Al_2O ratios strongly indicate chemical weathering and leaching (**B**). The upward decreasing Fe_2O_3/Al_2O_3 ratios suggest separation of Fe from Al. Chemical data from nodules, pebbles, and sulfates are excluded. Gray lines indicate the average values of Mars' crust.

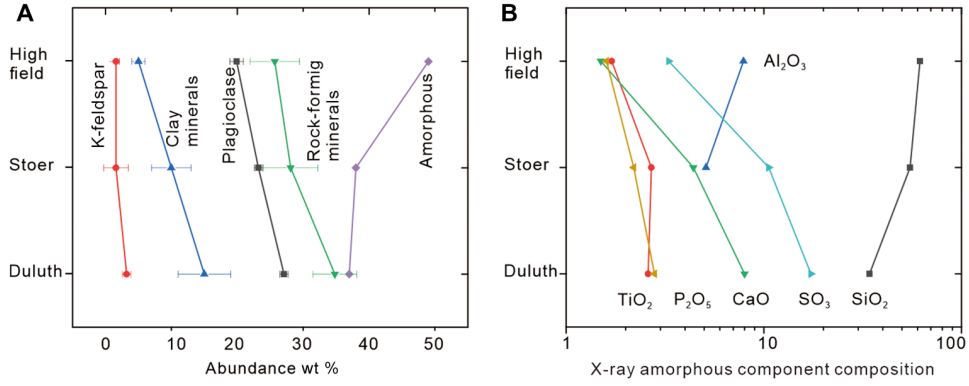

Fig. 4. Mineralogical evidence from chemical weathering. (**A**) Upward decreasing abundances of rock-forming minerals, plagioclase, K-feldspar, and phyllosilicates but increasing abundances of amorphous materials. (**B**) Upward decreasing trends of concentrations of SO_3, CaO, TiO_2, and P_2O_5 but increasing concentration of SiO_2 and Al_2O_3 in amorphous materials.

The weathering process is supported by decreasing abundances of rock-forming minerals and increasing abundances of amorphous components upward in the section (Fig. 4A). The upward increasing concentrations of SiO_2 in amorphous minerals (*34*) are also consistent with a weathering mechanism (Fig. 4B). The high concentrations of SiO_2 [up to 61.7 weight % (wt %)] with a little Al_2O_3 (0 to 7.9 wt %) in amorphous materials (*34*) are more consistent with acidic weathering products (*38*, *39*, *44*–*46*) than weathering products under a cold climate, which have a higher Al/Si ratio (*47*), e.g., allophane and/or imogolite (*48*, *49*). In addition, the clay mineralogy supports a weathering scenario. Clay minerals in the Duluth sample from the lower profile are mainly dominated by nontronite (*50*). Higher in the section, the nontronite itself might be weathered by acid fluid to form a 9.6-Å phyllosilicate with low layer charge (*5*, *34*). In the Highfield sample near the top of the section, there is less phyllosilicate overall and higher amorphous material (Fig. 4A) (*50*), which is consistent with acidic decomposition of both clay minerals and rock-forming minerals to form Si-rich amorphous materials (*38*, *39*, *44*–*46*, *51*). The mineralogical transitions are consistent with acidic hydrolysis and leaching during weathering. To summarize, lithological, geochemical, and mineralogical criteria are all indicative of a pedogenic weathering environment (*24*), but none of these trends are consistent with alteration in a closed basin lake.

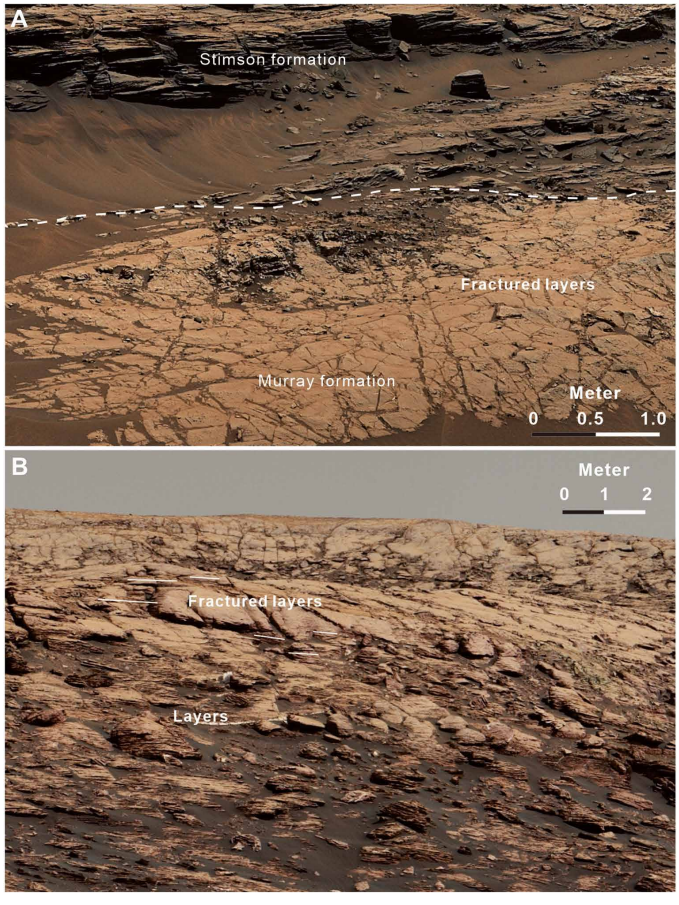

Fig. 5. Bleached, fractured clay-rich rocks underlying unconformity is similar with the uppermost part of VRR. (**A**) Bleached and fractured rocks (~0.2 m) directly below the unconformity show no evidence of lamination at the top of the Pahrump Hills member (Sol 992, mcam04393). (**B**) Laminations are clear in the lower sequence of VRR (Sol 1734, mcam09060). Some well-defined layers are laterally equivalent to fractured rock (~1 m in size) in the middle sequence. However, layering cannot be seen through fractures with the fracture patterns becoming intense and small (~0.2 m) in the upper sequence. The location of the sequence can be found in Fig. 1B.

The textural evidence for erosion, physical weathering, and leaching is demonstrated through several factors. First, clay-rich rocks from the Murray formation are unconformably overlain by eolian sandstone from the Stimson formation (Fig. 5A and fig. S7). The unconformity indicates sedimentary discontinuity, erosion, and weathering. The clay-rich rocks directly below the unconformity are bleached, fractured, and smooth and show no evidence of layered structures (Fig. 5A and fig. S7). However, there is a gradually upward transition from layered rocks to smooth and fractured rocks in the sequences at the Vera Rubin ridge (VRR) (Fig. 5B and fig. S8). The laminations, which are clear in lower sequence, were smoothed and broken into blocks around 1 m across in the middle sequence and around 0.2 m in the upper sequence. Layering can be seen through fractures in the middle sequence but cannot be seen in the upper sequence. The fractured patterns in the sequences are very similar in both size and shape to those observed below the unconformity at the top of the Pahrump Hills member (Fig. 5A). The gradual transition suggests that the layers were destroyed and fractured gradually because of top-down weathering. Physical erosion is also indicated by spherical weathering of layered structures (fig. S9A). The pores in siltstone of the Jura member indicate dissolution of crystalline minerals, which may result from chemical weathering and leaching (fig. S9B). The unconformity extends past VRR to the north and acts as a planal channel for accumulating diagenetic warm acidic water, which promotes the formation of crystalline hematite and preferentially hardened rocks (Fig. 6) (*50*–*52*). The pores formed by weathering also provide deposition spaces for crystallization of salts from diagenetic water (Fig. 6).

Owing to the high sulfur and chlorine abundances of the Mars' crust, the acidic surface water was generally sulfuric (*29*) and Cl rich. The top-down leaching contributed, at least partly, to the formation of sulfates (fig. S10A). The top-down leaching and deposition mechanism of sulfates explains why there are more sulfur and calcium in the lower sequence (fig. S11). It also accounts for why the Ca sulfates occur as veins cutting across layers with high angles in the middle weathering sequences but low angles in lower weathering sequences (fig. S3) (*13*, *31*). A leaching solution with abundant SO_4^{2-} and Ca crosscuts rocks higher in section; however, in the contact between the Blunts Point member and the Sutton island member, the fluid may have flowed laterally in a porous zone. This accounts for disseminated sulfates just above the contact (fig. S3D) (*31*).

A window into global-scale processes

A similarity in the remotely sensed spectral signature of clay minerals in Gale crater and Mawrth Vallis areas has been previously noted (*6*). Color patterns imaged by High Resolution Imaging Science Experiment (HiRISE) within the Gale crater weathering sequences are also similar to the weathering sequences in the Mawrth Vallis region (Fig. 7) (*11*). The blue patches in the upper sequences of the VRR profile and the Glen Torridon profile are known to be poor in Fe (and rich in Si and Al) based on in situ measurements (Fig. 8) (*29*, *33*). These fractured blue areas in upper sequence are similar to the Fe-poor blue horizons (*11*) remotely detected at Mawrth Vallis (Fig. 7), which are just below a dark mantle unit but above a

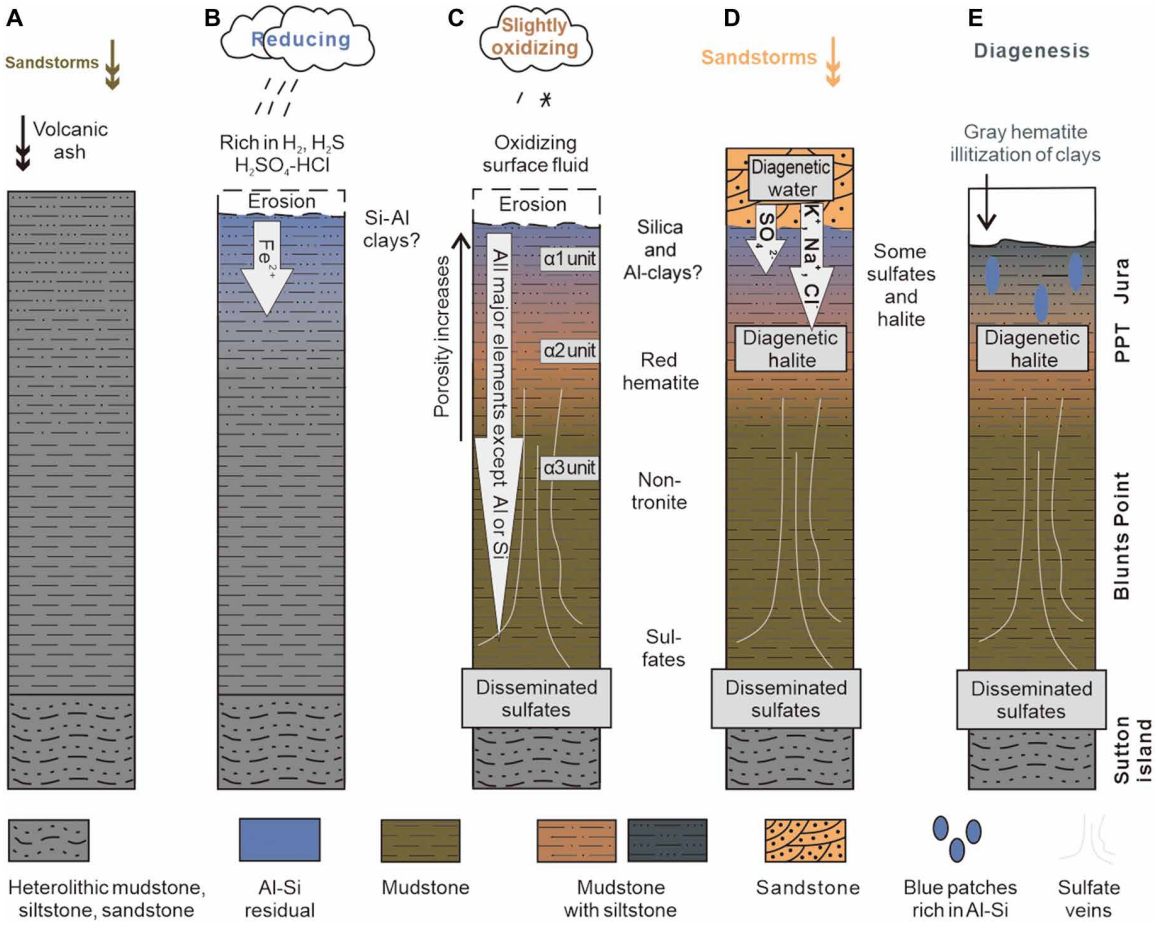

Fig. 6. Development of paleo-weathering sequences in Gale crater. (**A**) Airfall deposition of sediments with fine laminations and cross-bedding by volcanic and sandstorm events. (**B**) Anoxic weathering leached Fe and formed Al clays and silica-rich amorphous materials at the top section. (**C**) Physical weathering promotes erosion, and leaching causes porosity. Later, oxidizing water penetrated depth to form hematite and nontronite. Ca was leached to form veins that cut across layers with high angles in the middle section but low angles in the lower section and lastly occurs as bedding parallel veins and even disseminates in the bedrock around the contact between Sutton island. (**D**) Deposition of sand dunes of the Siccar Point group above VRR sequence. The mobile elements (e.g., Na and Cl) dissolved in the diagenetic water accumulated around the unconformity can penetrate deeper and occupy the pores and space created by weathering and leaching. It well explains why the sodium chloride mainly occurs in nodules and altered textures in the upper sequence (*32*). (**E**) Warm diagenesis around the unconformity promoted K-metasomatism and formation of gray hematite and sulfates (*65*). PPT, Pettegrove Point.

yellow-toned and layered unit (*53*, *54*). Infrared spectroscopic analyses showing a weathering trend of Fe depletion, Al enrichment, and hydroxylation of the weathering sequence upward in section are consistent with observations of a weathering sequence made by Curiosity (Fig. 8, B to E), providing an invaluable link between orbital and surface data. In other words, the clay mineral–bearing, blue-toned rocks observed from orbit at Gale crater are representative of a global process (Fig. 6), and the observations by Curiosity provide a window into fundamental, global-scale weathering processes on Mars (*55*).

Small-scale, saponite-magnetite–bearing mudstone deposits (*2*) at the lowest elevations in the floor of Gale crater are consistent with the occurrence of a shallow lake, but evidence for a large lake is lacking. The geochemical trends observed within hundreds of meters of stratigraphic section of sandstone-mudstone are more consistent with a continuous subaerial weathering sequence that formed in a reduced atmosphere, enabling Fe mobility in the Late Noachian to Early Hesperian (*11*). A fortunate outcome of the Curiosity mission is revelation of the details of a weathering pattern in situ that is observed by spectroscopic remote sensing both in Gale crater and throughout the ancient surface of Mars (*11*). The global climate transition was likely coupled to a transition in redox state, as Mars became colder, drier, and more oxidized in the Early Hesperian. The layered sulfates above the weathering sequences may form as a result of ice weathering (*56*–*59*) after the average temperature of Mars surface dropped below freezing point of water or the boundary between sulfate-dominated and clay-dominated weathering assemblages might represent a boundary between ice-dominated and meltwater-dominated weathering contexts.

MATERIALS AND METHODS

The concentrations of element oxides are obtained by the alpha particle x-ray spectrometer (APXS) on board the Curiosity rover. A description of the instrument, calibration methods, and data quantification can be found in (*60*), (*61*), and Planetary Data System (PDS) (*62*). The APXS is a contact instrument that uses Curium-244 sources to

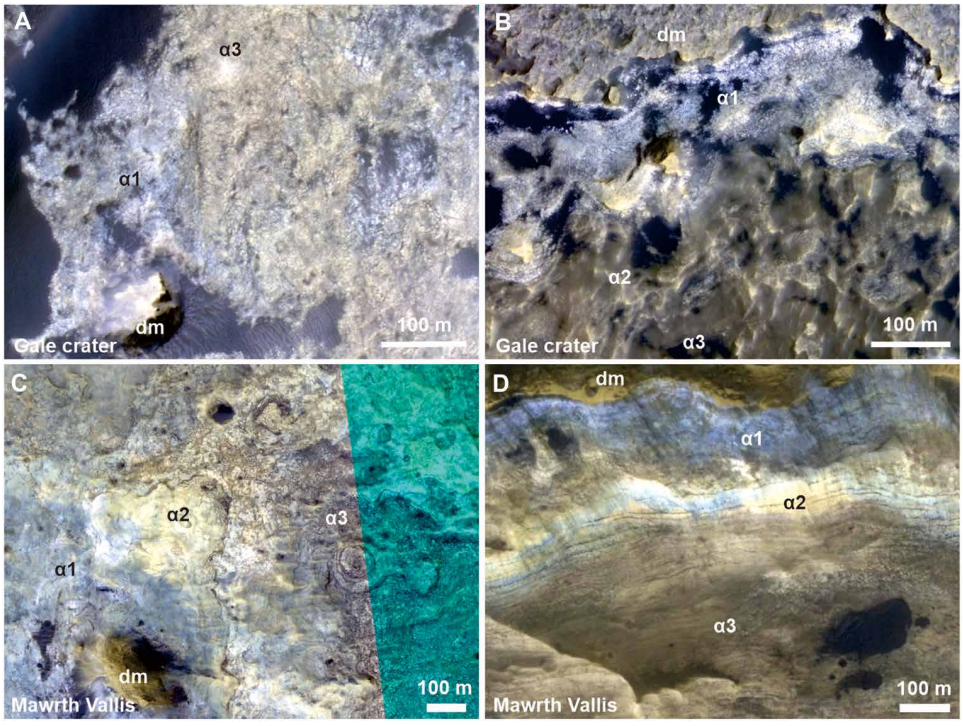

Fig. 7. HiRISE images of weathering sequences in Gale crater and Mawrth Vallis region. Weathering sequences in Gale crater (**A** and **B**) and Mawrth Vallis region (**C** and **D**) show the similar color patterns. The weathering sequences in both Gale crater and Mawrth Vallis region have Fe depleted bright blue-toned zone (α1 unit) and yellow-toned zone in the middle profiles (α2 unit) and a nontronite-dominant zone (α3 unit) in the lower sequences (*11*). In addition, the fracturation is more intense at upper sequences than those at lower sequence in Gale crater, which is also similar to Mawrth Vallis (*53*). (A) ESP_029034_1750_COLOR, (B) ESP_045293_1755_COLOR, (C) PSP_005819_2050_COLOR (*54*), and (D) ESP_012873_2045_COLOR (*11*, *53*). dm, dark mantle.

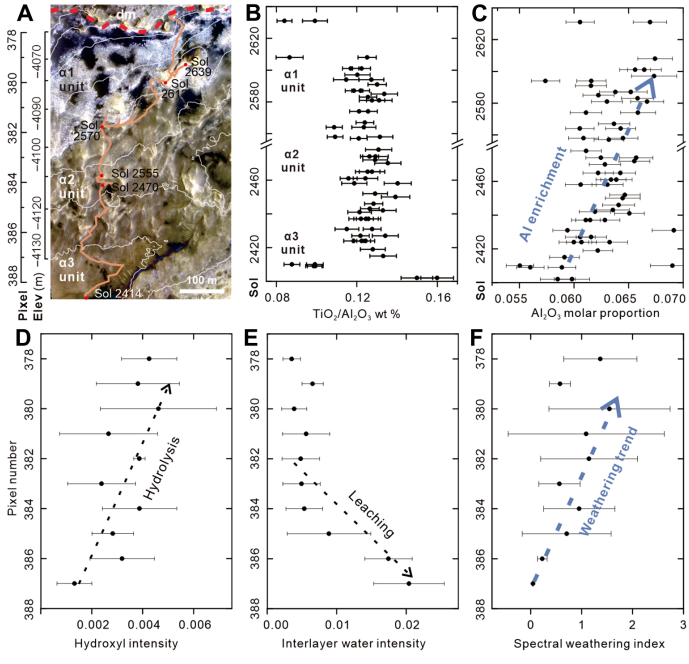

Fig. 8. Comparison between spectral and geochemical weathering index in the Glen Torridon region. (**A**) HiRISE image showing the Curiosity rover traverse from the dark brown Jura member to the bright yellow Knock Farril Hill member and, lastly, to the light blue-toned and fractured intermediated unit, which is just below unconformity (delineated by the red dashed line). (**B**) Constant TiO_2/Al_2O_3 ratio in the sequence. (**C**) Upward increasing trend of Al_2O_3 molar proportions with sol and elevation. The APXS data from Sol 2480 to Sol 2555 are not included, because there is no increase in elevation during that period. (**D**) Increasing trend of hydroxyl intensity (BD1400, hydrolysis degree). (**E**) Decreasing trend of interlayer water intensity (BD1900, leaching degree). (**F**) Increasing trend of spectral weathering index (BD1400/BD1900) (*11*, *63*).

Table 1. Abbreviations of reflectance spectral parameters. The meaning and calculation of (*a*) and (*b*) can be found from Viviano-Beck *et al.* (*66*). R#### indicates reflectance at a particular wavelength in nm.

Spectral index	Geological name	Calculation	Kernel width
BD1400	Hydroxyl intensity	1 – R1414/(*a**R1330 + *b**R1467)	R1330: 5, R1414: 7, R1467: 5
BD1900	Interlayer water intensity	1 – R1914/(*a**R1850 + *b**R2067)	R1850: 5, R1914: 3, R2067: 5
BD1400/BD1900	Weathering intensity	Ratio of BD1400 and BD1900	

induce particle-induced x-ray emission and x-ray fluorescence. The APXS spectra represent the average composition over the sampled area, which is ~1.7 cm in diameter when the instrument is in contact with the sample. All data used here are available on the PDS Geosciences Node (*62*). The sample descriptions and elevation information are thoroughly explained by Thompson *et al.* (*35*). Mineralogical abundances used here are obtained from XRD measurements using Curiosity's CheMin instrument. A complete description of the instrument and the calibration methods and the quantification of XRD data can be found in Bristow *et al.* (*5*) and Rampe *et al.* (*34*, *50*). Mineralogical abundances are from Rampe *et al.* (*34*, *50*). Amorphous composition and abundance are from Rampe *et al.* (*34*).

The formulas of BD1400 and BD1900 and their ratio are from Liu *et al.* (*11*, *63*). To eliminate the influence of absorbed water on the value of BD1900 of water complexes created by alkaline elements, the absorption of absorbed water around 1985 nm is excluded in its formula. The central wavelengths and wider kernel width for BD1400 and BD1900 are selected according to the wavelength of the absorption minimum of hydrated minerals in the area, which mainly located at ~1421 and ~1914 nm, respectively. Different selections of the central wavelength of absorption around 1400 and 1900 nm do not influence the trend of BD1400/BD1900 value. The detailed calculation processes are listed in Table 1. We first calculate spectral parameters of single spectrum (1 × 1 pixel) and then calculate their mean value at the same elevation (1 × 3 pixels) and SD. The error is likely from some inevitable sand cover in the weathering sequence, which renders the error a little large.

SUPPLEMENTARY MATERIALS

Supplementary material for this article is available at http://advances.sciencemag.org/cgi/content/full/7/32/eabh2687/DC1

REFERENCES AND NOTES

1. J. A. Hurowitz, J. P. Grotzinger, W. W. Fischer, S. M. McLennan, R. E. Milliken, N. Stein, A. R. Vasavada, D. F. Blake, E. Dehouck, J. L. Eigenbrode, A. G. Fairén, J. Frydenvang, R. Gellert, J. A. Grant, S. Gupta, K. E. Herkenhoff, D. W. Ming, E. B. Rampe, M. E. Scmidt, K. L. Siebach, K. Stack-Morgan, D. Y. Sumner, R. C. Wiens, Redox stratification of an ancient lake in Gale crater, Mars. *Science* **356**, eaah6849 (2017).
2. D. T. Vaniman, D. L. Bish, D. W. Ming, T. F. Bristow, R. V. Morris, D. F. Blake, S. J. Chipera, S. M. Morrison, A. H. Treiman, E. B. Rampe, M. Rice, C. N. Achilles, J. P. Grotzinger, S. M. McLennan, J. Williams, J. F. Bell III, H. E. Newsom, R. T. Downs, S. Maurice, P. Sarrazin, A. S. Yen, J. M. Morookian, J. D. Farmer, K. Stack, R. E. Milliken, B. L. Ehlmann, D. Y. Sumner, G. Berger, J. A. Crisp, J. A. Hurowitz, R. Anderson, D. J. Des Marais, E. M. Stolper, K. S. Edgett, S. Gupta, N. Spanovich; MSL Science Team, Mineralogy of a mudstone at Yellowknife Bay, Gale crater, Mars. *Science* **343**, 1243480 (2014).
3. J. P. Grotzinger, D. Y. Sumner, L. C. Kah, K. Stack, S. Gupta, L. Edgar, D. Rubin, K. Lewis, J. Schieber, N. Mangold, R. Milliken, P. G. Conrad, D. DesMarais, J. Farmer, K. Siebach, F. Calef, J. Hurowitz, S. M. McLennan, D. Ming, D. Vaniman, J. Crisp, A. Vasavada, K. S. Edgett, M. Malin, D. Blake, R. Gellert, P. Mahaffy, R. C. Wiens, S. Maurice, J. A. Grant, S. Wilson, R. C. Anderson, L. Beegle, R. Arvidson, B. Hallet, R. S. Sletten, M. Rice, J. Bell, J. Griffes, B. Ehlmann, R. B. Anderson, T. F. Bristow, W. E. Dietrich, G. Dromart, J. Eigenbrode, A. Fraeman, C. Hardgrove, K. Herkenhoff, L. Jandura, G. Kocurek, S. Lee, L. A. Leshin, R. Leveille, D. Limonadi, J. Maki, S. McCloskey, M. Meyer, M. Minitti, H. Newsom, D. Oehler, A. Okon, M. Palucis, T. Parker, S. Rowland, M. Schmidt, S. Squyres, A. Steele, E. Stolper, R. Summons, A. Treiman, R. Williams, A. Yingst; MSL Science Team, A habitable fluvio-lacustrine environment at Yellowknife Bay, Gale crater, Mars. *Science* **343**, 1242777 (2014).
4. J. P. Grotzinger, S. Gupta, M. C. Malin, D. M. Rubin, J. Schieber, K. Siebach, D. Y. Sumner, K. M. Stack, A. R. Vasavada, R. E. Arvidson, F. Calef, L. Edgar, W. F. Fischer, J. A. Grant, J. Griffes, L. C. Kah, M. P. Lamb, K. W. Lewis, N. Mangold, M. E. Minitti, M. Palucis, M. Rice, R. M. E. Williams, R. A. Yingst, D. Blake, D. Blaney, P. Conrad, J. Crisp, W. E. Dietrich, G. Dromart, K. S. Edgett, R. C. Ewing, R. Gellert, J. A. Hurowitz, G. Kocurek, P. Mahaffy, M. J. McBride, S. M. McLennan, M. Mischna, D. Ming, R. Milliken, H. Newsom, D. Oehler, T. J. Parker, D. Vaniman, R. C. Wiens, S. A. Wilson, Deposition, exhumation, and paleoclimate of an ancient lake deposit, Gale crater, Mars. *Science* **350**, aac7575 (2015).
5. T. F. Bristow, E. B. Rampe, C. N. Achilles, D. F. Blake, S. J. Chipera, P. Craig, J. A. Crisp, D. J. Des Marais, R. T. Downs, R. Gellert, J. P. Grotzinger, S. Gupta, R. M. Hazen, B. Horgan, J. V. Hogancamp, N. Mangold, P. R. Mahaffy, A. C. McAdam, D. W. Ming, J. M. Morookian, R. V. Morris, S. M. Morrison, A. H. Treiman, D. T. Vaniman, A. R. Vasavada, A. S. Yen, Clay mineral diversity and abundance in sedimentary rocks of Gale crater, Mars. *Sci. Adv.* **4**, eaar3330 (2018).
6. B. J. Thomson, D. L. Buczkowski, L. S. Crumpler, K. D. Seelos, C. I. Fassett, How much of the sediment in Gale crater's central mound was fluvially transported? *Geophys. Res. Lett.* **46**, 5092–5099 (2019).
7. M. C. Palucis, W. E. Dietrich, R. M. E. Williams, A. G. Hayes, T. Parker, D. Y. Sumner, N. Mangold, K. Lewis, H. Newsom, Sequence and relative timing of large lakes in Gale crater (Mars) after the formation of Mount Sharp. *J. Geophys. Res. Planets.* **121**, 472–496 (2016).
8. R. E. Milliken, J. P. Grotzinger, B. J. Thomson, Paleoclimate of Mars as captured by the stratigraphic record in Gale Crater. *Geophys. Res. Lett.* **37**, L04201 (2010).
9. E. S. Kite, K. W. Lewis, M. P. Lamb, C. E. Newman, M. I. Richardson, Growth and form of the mound in Gale Crater, Mars: Slope wind enhanced erosion and transport. *Geology* **41**, 543–546 (2013).
10. B. J. Thomson, N. T. Bridges, R. Milliken, A. Baldridge, S. J. Hook, J. K. Crowley, G. M. Marion, C. R. de Souza, A. J. Brown, C. M. Weitz, Constraints on the origin and evolution of the layered mound in Gale Crater, Mars using Mars Reconnaissance Orbiter data. *Icarus* **214**, 413–432 (2011).
11. J. Liu, J. R. Michalski, W. Tan, H. He, B. Ye, L. Xiao, Anoxic chemical weathering under a reducing greenhouse on early Mars. *Nat. Astron.* **5**, 503–509 (2021).
12. R. M. E. Williams, J. P. Grotzinger, W. E. Dietrich, S. Gupta, D. Y. Sumner, R. C. Wiens, N. Mangold, M. C. Malin, K. S. Edgett, S. Maurice, O. Forni, O. Gasnault, A. Ollila, H. E. Newsom, G. Dromart, M. C. Palucis, R. A. Yingst, R. B. Anderson, K. E. Herkenhoff, S. Le Mouélic, W. Goetz, M. B. Madsen, A. Koefoed, J. K. Jensen, J. C. Bridges, S. P. Schwenzer, K. W. Lewis, K. M. Stack, D. Rubin, L. C. Kah, J. F. Bell, J. D. Farmer, R. Sullivan, T. Van Beek, D. L. Blaney, O. Pariser, R. G. Deen, M. S. L. S. Team, Martian fluvial conglomerates at gale crater. *Science* **340**, 1068–1072 (2013).
13. L. A. Edgar, C. M. Fedo, S. Gupta, S. G. Banham, A. A. Fraeman, J. P. Grotzinger, K. M. Stack, N. T. Stein, K. A. Bennett, F. Rivera-Hernández, V. Z. Sun, K. S. Edgett, D. M. Rubin, C. House, J. Van Beek, A lacustrine paleoenvironment recorded at Vera RubinRidge, Gale crater: Overview of the sedimentology and stratigraphy observed by the Mars Science Laboratory Curiosity Rover. *J. Geophys. Res. Planets.* **125**, e2019JE006307 (2020).
14. N. T. Stein, D. P. Quinn, J. P. Grotzinger, C. Fedo, B. L. Ehlmann, K. M. Stack, L. A. Edgar, A. A. Fraeman, R. Deen, Regional structural orientation of the Mount Sharp group revealed by in situ dip measurements and stratigraphic correlations on the Vera Rubin ridge. *J. Geophys. Res. Planets.* **125**, e2019JE006298 (2020).
15. R. V. Morris, E. B. Rampe, D. T. Vaniman, R. Christoffersen, A. S. Yen, S. M. Morrison, D. W. Ming, C. N. Achilles, A. A. Fraeman, L. Le, V. M. Tu, J. P. Ott, A. H. Treiman, J. V. Hogancamp, T. G. Graff, M. Adams, J. C. Hamilton, S. A. Mertzman, T. F. Bristow, D. F. Blake, N. Castle, S. J. Chipera, P. I. Craig, D. J. Des Marais, G. Downs, R. T. Downs,

R. M. Hazen, J.-M. Morookian, M. Thorpe, Hydrothermal precipitation of sanidine (adularia) having full Al, Si structural disorder and specular hematite at Maunakea volcano (Hawai'i) and at Gale Crater (Mars). *J. Geophys. Res. Planets.* **125**, e2019JE006324 (2020).
16. A. S. Yen, R. V Morris, D. W. Ming, S. P. Schwenzer, B. Sutter, D. T. Vaniman, A. H. Treiman, R. Gellert, C. N. Achilles, J. A. Berger, D. F. Blake, N. I. Boyd, T. F. Bristow, S. Chipera, B. C. Clark, P. I. Craig, R. T. Downs, H. B. Franz, T. Gabriel, A. C. McAdam, S. M. Morrison, C. D. O'Connell-Cooper, E. B. Rampe, M. E. Schmidt, L. M. Thompson, S. J. VanBommel, Formation of tridymite and evidence for a hydrothermal history at Gale Crater. *Mars. J. Geophys. Res. Planets* **126**, e2020JE006569 (2020).
17. J. A. Berger, M. E. Schmidt, R. Gellert, N. I. Boyd, E. D. Desouza, R. L. Flemming, M. R. M. Izawa, D. W. Ming, G. M. Perrett, E. B. Rampe, L. M. Thompson, S. J. V. VanBommel, A. S. Yen, Zinc and germanium in the sedimentary rocks of Gale Crater on Mars indicate hydrothermal enrichment followed by diagenetic fractionation. *J. Geophys. Res. Planets.* **122**, 1747–1772 (2017).
18. N. Mangold, E. Dehouck, C. Fedo, O. Forni, C. Achilles, T. Bristow, R. T. Downs, J. Frydenvang, O. Gasnault, J. L'haridon, L. Le Deit, S. Maurice, S. M. McLennan, P.-Y. Meslin, S. Morrison, H. E. Newsom, E. Rampe, W. Rapin, F. Rivera-Hernandez, M. Salvatore, R. C. Wiens, Chemical alteration of fine-grained sedimentary rocks at Gale crater. *Icarus* **321**, 619–631 (2019).
19. J. Frydenvang, N. Mangold, R. C. Wiens, A. A. Fraeman, L. A. Edgar, C. M. Fedo, J. L'Haridon, C. C. Bedford, S. Gupta, J. P. Grotzinger, J. C. Bridges, B. C. Clark, E. B. Rampe, O. Gasnault, S. Maurice, P. J. Gasda, N. L. Lanza, A. M. Olilla, P.-Y. Meslin, V. Payré, F. Calef, M. Salvatore, C. H. House, The chemostratigraphy of the Murray formation and role of diagenesis at Vera Rubin ridge in Gale crater, Mars, as observed by the ChemCam instrument. *J. Geophys. Res. Planets.* **125**, e2019JE006320 (2020).
20. S. M. McLennan, E. Dehouck, J. P. Grotzinger, J. A. Hurowitz, N. Mangold, K. Siebach, Geochemical record of open-system chemical weathering at Gale Crater and implications for paleoclimates on Mars, in *46th Lunar and Planetary Science Conference*, 16 to 20 March 2015.
21. K. L. Siebach, S. M. McLennan, Re-Evaluating the CIA paleoclimate proxy on Mars at Curiosity's drill sites, in *49th Lunar and Planetary Science Conference*, 19 to 23 March 2018.
22. M. T. Thorpe, J. A. Hurowitz, K. L. Siebach, Source-to-sink terrestrial analogs for the paleoenvironment of Gale crater, Mars. *J. Geophys. Res. Planets* **126**, e2020JE006530 (2021).
23. K. L. Siebach, C. N. Achilles, R. J. Smith, S. M. McLennan, E. Dehouck, Using Curiosity Drill Sites to Test the Chemical Index of Alteration, in *51th Lunar and Planetary Science Conference*, 16 to 20 March 2020.
24. H. W. Nesbitt, G. M. Young, Early proterozoic climates and plate motions inferred from major element chemistry of lutites. *Nature* **299**, 715–717 (1982).
25. J. A. Hurowitz, S. M. McLennan, N. J. Tosca, R. E. Arvidson, J. R. Michalski, D. W. Ming, C. Schröder, S. W. Squyres, In situ and experimental evidence for acidic weathering of rocks and soils on Mars. *J. Geophys. Res. E Planets.* **111**, E02S19 (2006).
26. H. Y. McSween Jr., Petrology on Mars. *Am. Mineral.* **100**, 2380–2395 (2015).
27. E. M. Hausrath, A. K. Navarre-Sitchler, P. B. Sak, C. I. Steefel, S. L. Brantley, Basalt weathering rates on Earth and the duration of liquid water on the plains of Gusev Crater, Mars. *Geology* **36**, 67–70 (2008).
28. J. A. Hurowitz, W. W. Fischer, N. J. Tosca, R. E. Milliken, Origin of acidic surface waters and the evolution of atmospheric chemistry on early Mars. *Nat. Geosci.* **3**, 323–326 (2010).
29. J. A. Hurowitz, S. M. McLennan, A ~3.5 Ga record of water-limited, acidic weathering conditions on Mars. *Earth Planet. Sci. Lett.* **260**, 432–443 (2007).
30. M. Y. Zolotov, M. V. Mironenko, Chemical models for martian weathering profiles: Insights into formation of layered phyllosilicate and sulfate deposits. *Icarus* **275**, 203–220 (2016).
31. W. Rapin, B. L. Ehlmann, G. Dromart, J. Schieber, N. H. Thomas, W. W. Fischer, V. K. Fox, N. T. Stein, M. Nachon, B. C. Clark, L. C. Kah, L. Thompson, H. A. Meyer, T. S. J. Gabriel, C. Hardgrove, N. Mangold, F. Rivera-Hernandez, R. C. Wiens, A. R. Vasavada, An interval of high salinity in ancient Gale crater lake on Mars. *Nat. Geosci.* **12**, 889–895 (2019).
32. N. H. Thomas, B. L. Ehlmann, P. Meslin, W. Rapin, D. E. Anderson, F. Rivera-Hernández, O. Forni, S. Schröder, A. Cousin, N. Mangold, R. Gellert, O. Gasnault, R. C. Wiens, Mars Science Laboratory observations of chloride salts in Gale Crater, Mars. *Geophys. Res. Lett.* **46**, 10754–10763 (2019).
33. C. M. Fedo, H. Wayne Nesbitt, G. M. Young, Unraveling the effects of potassium metasomatism in sedimentary rocks and paleosols, with implications for paleoweathering conditions and provenance. *Geology* **23**, 921–924 (1995).
34. E. B. Rampe, D. F. Blake, T. F. Bristow, D. W. Ming, D. T. Vaniman, R. V. Morris, C. N. Achilles, S. J. Chipera, S. M. Morrison, V. M. Tu, A. S. Yen, N. Castle, G. W. Downs, R. T. Downs, J. P. Grotzinger, R. M. Hazen, A. H. Treiman, T. S. Peretyazhko, D. J. D. Marais, R. C. Walroth, P. I. Craig, J. A. Crisp, B. Lafuente, J. M. Morookian, P. C. Sarrazin, M. T. Thorpe, J. C. Bridges, L. A. Edgar, C. M. Fedo, C. Freissinet, R. Gellert, P. R. Mahaffy, H. E. Newsom, J. R. Johnson, L. C. Kah, K. L. Siebach, J. Schieber, V. Z. Sun, A. R. Vasavada, D. Wellington, R. C. Wiens, Mineralogy and geochemistry of sedimentary rocks and eolian sediments in Gale crater, Mars: A review after six Earth years of exploration with Curiosity. *Geochemistry* **80**, 125605 (2020).
35. L. M. Thompson, J. A. Berger, J. G. Spray, A. A. Fraeman, M. A. McCraig, C. D. O'Connell-Cooper, M. E. Schmidt, S. VanBommel, R. Gellert, A. Yen, N. I. Boyd, APXS-derived compositional characteristics of Vera Rubin Ridge and Murray formation, Gale crater, Mars: Geochemical implications for the origin of the ridge. *J. Geophys. Res. Planets.* **125**, e2019JE006319 (2020).
36. S. M. McLennan, Sedimentary silica on Mars. *Geology* **31**, 315–318 (2003).
37. W. L. Marshall, J. M. Warakomski, Amorphous silica solubilities—II. Effect of aqueous salt solutions at 25°C. *Geochim. Cosmochim. Acta* **44**, 915–924 (1980).
38. R. J. Smith, B. H. N. Horgan, P. Mann, E. A. Cloutis, P. R. Christensen, Acid weathering of basalt and basaltic glass: 2. Effects of microscopic alteration textures on spectral properties. *J. Geophys. Res. Planets.* **122**, 203–227 (2017).
39. B. H. N. Horgan, R. J. Smith, E. A. Cloutis, P. Mann, P. R. Christensen, Acidic weathering of basalt and basaltic glass: 1. Near-infrared spectra, thermal infrared spectra, and implications for Mars. *J. Geophys. Res. Planets.* **122**, 172–202 (2017).
40. T. S. Peretyazhko, P. B. Niles, B. Sutter, R. V. Morris, D. G. Agresti, L. Le, D. W. Ming, Smectite formation in the presence of sulfuric acid: Implications for acidic smectite formation on early Mars. *Geochim. Cosmochim. Acta* **220**, 248–260 (2018).
41. T. S. Peretyazhko, B. Sutter, R. V. Morris, D. G. Agresti, L. Le, D. W. Ming, Fe/Mg smectite formation under acidic conditions on early Mars. *Geochim. Cosmochim. Acta* **173**, 37–49 (2016).
42. M. Y. Zolotov, M. V. Mironenko, Timing of acid weathering on Mars: A kinetic-thermodynamic assessment. *J. Geophys. Res. E Planets* **112**, E07006 (2007).
43. R. Rye, H. D. Holland, Paleosols and the evolution of atmospheric oxygen: A critical review. *Am. J. Sci.* **298**, 621–672 (1998).
44. J. Madejová, M. Pentrák, H. Pálková, P. Komadel, Near-infrared spectroscopy: A powerful tool in studies of acid-treated clay minerals. *Vib. Spectrosc.* **49**, 211–218 (2009).
45. P. Komadel, D. Schmidt, J. Madejová, B. Cˇíceˇl, Alteration of smectites by treatments with hydrochloric acid and sodium carbonate solutions. *Appl. Clay Sci.* **5**, 113–122 (1990).
46. P. Komadel, Acid activated clays: Materials in continuous demand. *Appl. Clay Sci.* **131**, 84–99 (2016).
47. K. Wada, Minerals formed and mineral formation from volcanic ash by weathering. *Chem. Geol.* **60**, 17–28 (1987).
48. J. L. Bishop, A. G. Fairén, J. R. Michalski, L. Gago-Duport, L. L. Baker, M. A. Velbel, C. Gross, E. B. Rampe, Surface clay formation during short-term warmer and wetter conditions on a largely cold ancient Mars. *Nat. Astron.* **2**, 206–213 (2018).
49. J. L. Bishop, E. B. Rampe, Evidence for a changing Martian climate from the mineralogy at Mawrth Vallis. *Earth Planet. Sci. Lett.* **448**, 42–48 (2016).
50. E. B. Rampe, T. F. Bristow, R. V. Morris, S. M. Morrison, C. N. Achilles, D. W. Ming, D. T. Vaniman, D. F. Blake, V. M. Tu, S. J. Chipera, A. S. Yen, T. S. Peretyazhko, R. T. Downs, R. M. Hazen, A. H. Treiman, J. P. Grotzinger, N. Castle, P. I. Craig, D. J. D. Marais, M. T. Thorpe, R. C. Walroth, G. W. Downs, A. A. Fraeman, K. L. Siebach, R. Gellert, B. Lafuente, A. C. McAdam, P.-Y. Meslin, B. Sutter, M. R. Salvatore, Mineralogy of Vera Rubin Ridge from the Mars Science Laboratory CheMin Instrument. *J. Geophys. Res. Planets.* **125**, e2019JE006306 (2020).
51. P. I. Craig, D. W. Ming, E. B. Rampe, R. V. Morris, Sulfate mineral formation from acid-weathered phyllosilicates: Implications for the aqueous history of Mars, in *46th Lunar and Planetary Science Conference*, 16 to 20 March 2015.
52. G. David, A. Cousin, O. Forni, P. -Y. Meslin, E. Dehouck, N. Mangold, J. L'Haridon, W. Rapin, O. Gasnault, J. R. Johnson, A. M. Ollila, A. R. Newell, M. Salvatore, T. S. J. Gabriel, R. C. Wiens, S. Maurice, Analyses of high-iron sedimentary bedrock and diagenetic features observed with ChemCam at Vera Rubin ridge, Gale crater, Mars: Calibration and characterization. *J. Geophys. Res. Planets.* **125**, e2019JE006314 (2020).
53. D. R. Lowe, J. L. Bishop, D. Loizeau, J. J. Wray, R. A. Beyer, Deposition of >3.7 Ga clay-rich strata of the Mawrth Vallis Group, Mars, in lacustrine, alluvial, and aeolian environments. *GSA Bull.* **132**, 17–30 (2020).
54. S. L. Murchie, J. F. Mustard, B. L. Ehlmann, R. E. Milliken, J. L. Bishop, N. K. McKeown, E. Z. Noe Dobrea, F. P. Seelos, D. L. Buczkowski, S. M. Wiseman, R. E. Arvidson, J. J. Wray, G. Swayze, R. N. Clark, D. J. Des Marais, A. S. McEwen, J. P. Bibring, A synthesis of Martian aqueous mineralogy after 1 Mars year of observations from the Mars Reconnaissance Orbiter. *J. Geophys. Res. E Planets.* **114**, E00D06 (2009).
55. J. Carter, D. Loizeau, N. Mangold, F. Poulet, J. P. Bibring, Widespread surface weathering on early Mars: A case for a warmer and wetter climate. *Icarus* **248**, E00D06 (2014).
56. P. B. Niles, J. Michalski, Meridiani Planum sediments on mars formed through weathering in massive ice deposits. *Nat. Geosci.* **2**, 215–220 (2009).
57. P. B. Niles, J. Michalski, D. W. Ming, D. C. Golden, Elevated olivine weathering rates and sulfate formation at cryogenic temperatures on Mars. *Nat. Commun.* **8**, 998 (2017).

58. J. Michalski, P. B. Niles, Atmospheric origin of martian interior layered deposits: Links to climate change and the global sulfur cycle. *Geology* **40**, 419–422 (2012).
59. G. Baccolo, B. Delmonte, P. B. Niles, G. Cibin, E. Di Stefano, D. Hampai, L. Keller, V. Maggi, A. Marcelli, J. Michalski, C. Snead, M. Frezzotti, Jarosite formation in deep Antarctic ice provides a window into acidic, water-limited weathering on Mars. *Nat. Commun.* **12**, 436 (2021).
60. R. Gellert, R. Rieder, J. Brückner, B. C. Clark, G. Dreibus, G. Klingelhöfer, G. Lugmair, D. W. Ming, H. Wänke, A. Yen, J. Zipfel, S. W. Squyres, Alpha Particle X-ray Spectrometer (APXS): Results from Gusev crater and calibration report. *J. Geophys. Res. Planets.* **111**, E02S05 (2006).
61. J. L. Campbell, G. M. Perrett, R. Gellert, S. M. Andrushenko, N. I. Boyd, J. A. Maxwell, P. L. King, C. D. M. Schofield, Calibration of the Mars Science Laboratory alpha particle x-ray spectrometer. *Space Sci. Rev.* **170**, 319–340 (2012).
62. R. Gellert, Mars Science Laboratory Alpha Particle X-Ray Spectrometer RDR data V1.0, MSL-M-APXS-4/5-RDR-V1.0 (NASA Planetary Data System, 2013).
63. J. C. Liu, H. P. He, J. Michalski, C. Javier, Y. Z. Yao, W. Tan, X. R. Qin, S. Y. Li, G. J. Wei, Reflectance spectroscopy applied to clay mineralogy and alteration intensity of a thick basaltic weathering sequence in Hainan Island, South China. *Appl. Clay Sci.* **201**, 105923 (2021).
64. C. Fedo, J. P. Grotzinger, S. Gupta, S. Banham, K. Bennett, L. Edgar, V. Fox, A. Fraeman, C. House, K. Lewis, K. M. Stack, D. Rubin, K. Siebach, D. Sumner, V. Sun, A. Vasavada, Evidence for persistent, water-rich, lacustrine deposition preserved in the Murray formation, Gale crater: A depositional system suitable for sustained habitability, in *Ninth International Conference on Mars*, 15 to 19 July 2019.
65. P. Craig, D. Ming, E. Rampe, Sulfate Formation From Acid-Weathered Phylosilicates: Implications for the Aqueous History of Mars, in *Eighth International Conference on Mars*, 14 to 18 July 2019.
66. C. E. Viviano-Beck, F. P. Seelos, S. L. Murchie, E. G. Kahn, K. D. Seelos, H. W. Taylor, K. Taylor, B. L. Ehlmann, S. M. Wisemann, J. F. Mustard, M. F. Morgan, Revised CRISM spectral parameters and summary products based on the currently detected mineral diversity on Mars. *J. Geophys. Res. Planets.* **119**, 1403–1431 (2014).

Acknowledgments: We are grateful to those MSL team members and MSL project's engineering and management teams. We also acknowledge help from Z. Liu and Y. Song for software operation. We thank W. Shen for discussion and M. Y. H. Li and C. L. K. Chak for revision. **Funding:** This work was funded by the Research Grants Council General Research Fund to J.R.M. (grant number 17307417). **Author contributions:** J.L. carried out all geochemical and mineralogical analyses and wrote the manuscript. J.R.M. conceptualized the project and helped write the paper. M.-F.Z. contributed to the discussion of content and revisions of the manuscript. **Competing interests:** The authors declare that they have no competing interests. **Data and materials availability:** All data needed to evaluate the conclusions in the paper are present in the paper and/or the Supplementary Materials. Data obtained by the Curiosity rover are archived in the PDS at http://pds-geosciences.wustl.edu/missions/msl/index.htm. Additional data related to this paper may be requested from the authors.

Submitted 25 February 2021
Accepted 21 June 2021
Published 6 August 2021
10.1126/sciadv.abh2687

Citation: J. Liu, J. R. Michalski, M.-F. Zhou, Intense subaerial weathering of eolian sediments in Gale crater, Mars. *Sci. Adv.* **7**, eabh2687 (2021).